

Surface Roughness Effect in Hydrodynamic Thrust Bearing with Ultra Low Clearance

Chao Wang⁽¹⁾, Yongbin Zhang^(1,*)

⁽¹⁾ College of Mechanical Engineering, Changzhou University, Changzhou, Jiangsu Province, CHINA

^(*) Corresponding author, e-mail: engmech1@sina.com

SUMMARY

In the hydrodynamic thrust bearing with ultra-low clearance, even the nanoscale surface roughness is comparable to the bearing clearance, and its effect can be very significant. In this paper, the calculations are made for the performance of this bearing when the surface roughness is on the 1nm scale. It was found that the surface roughness effect in the bearing is strongly dependent on the physical adsorption of the fluid to the bearing surface determined by the interaction strength (or potential) between the fluid molecules and the molecules of the bearing surface; it can considerably enhance the load-carrying capacity of the bearing for the strong interaction between the fluid and the bearing surfaces.

KEY WORDS: bearing; boundary layer; hydrodynamics; multiscale; surface roughness.

1. INTRODUCTION

In harsh conditions, there will be a very small or even ultra-small surface clearance in a hydrodynamic thrust bearing [1-3]. In a micro thrust bearing, the clearance is also intrinsically very small [4]. In these two circumstances, the influence of the fluid molecule layers on the bearing surfaces ought to be considered [5-7]. Depending on the physical adsorption of the fluid to the bearing surface, the adhering layer is highly solidified or flows with certain mobility [8-10]. With the lubricant of long-chain molecules, the adhering layer is considered the solid layer [11], [12]. However, in thrust bearings of small sizes, the lubricant is usually simple fluid such as water, alcohol, acetone, etc. These fluids still possess flow ability adjacent to the bearing surface. For the thrust bearing with ultra-low clearance, the multiscale hydrodynamic analysis should thus be required by considering the flows of both the adsorbed layers and the continuum fluid.

We made multiscale analyses and numerical calculations for the hydrodynamic thrust bearing with ultra/low clearance when both bearing surfaces were perfectly smooth [13]. New results were obtained concerning the strong influence of the adsorbed layer on the performance of this bearing. However, there is still important research to be done on the surface roughness effect of

this bearing since the nanoscale surface roughness is on the same scale as the bearing clearance. In practice, the surface roughness in a bearing is much larger than the nanoscale size, and the surface roughness effect is expected to be very significant.

This paper studies the surface roughness effect in the hydrodynamic thrust bearing with ultra/low clearance with the multiscale approach when the stationary bearing surface is imposed with the sinusoidal surface roughness and the moving bearing surface is assumed to be perfectly smooth. The surface roughness is taken on the 1nm scale. Even in this case, the lubrication status in the bearing is quite complex with irregularly distributed boundary films and intervening continuum fluid films. The numerical calculation was carried out by forward difference to solve the one-order differential equation. Important findings were obtained on how the surface roughness effect plays in the studied bearing.

2. HYDRODYNAMIC THRUST BEARING WITH ULTRA/LOW CLEARANCE AND NANOSCALE SURFACE ROUGHNESS

The hydrodynamic thrust bearing with ultralow clearance is shown in Figure 1, where the moving surface with the speed u , is assumed as perfectly smooth, and the stationary surface with the sinusoidal nanoscale surface roughness. Besides the very thin layer adhering to the whole surface, the intermediate continuum fluid film is distributed depending on the surface clearance and roughness. The lubrication status is complex, so different equations should be used for the zones of different lubrication regimes.

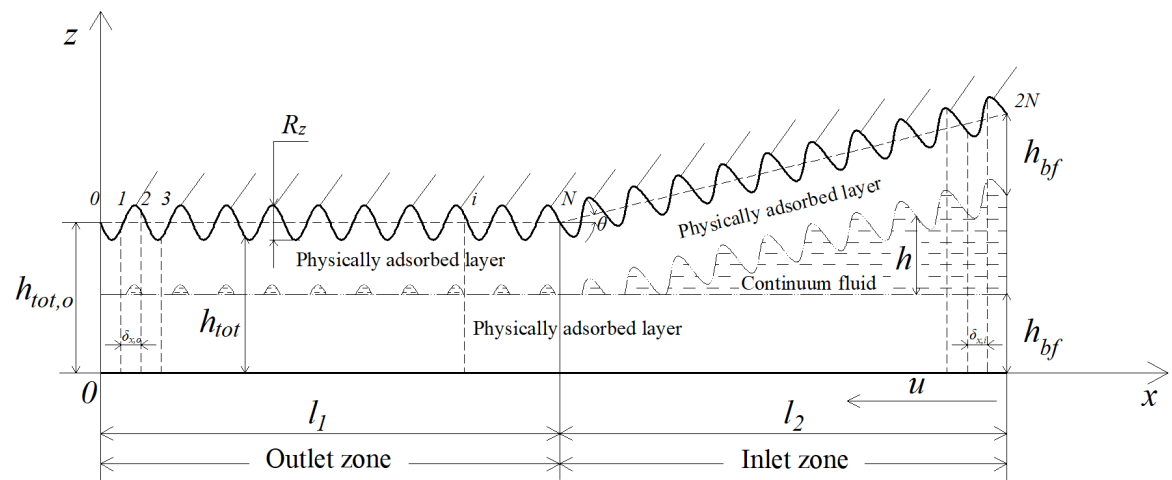


Fig. 1 The studied hydrodynamic thrust bearing with ultra-low clearance and imposed nanoscale surface roughness

3. ANALYSIS

The multiscale analysis should be used for evaluating the performance of the bearing in Figure 1, considering the flows of both the adsorbed layer and the continuum fluid. When the adsorbed layer and the continuum fluid coexist, the multiscale flow equations developed by Zhang [14] are used. When only the adsorbed layer exists, the nanoscale non-continuum flow equation [15] is used.

In the analysis, the following assumptions were made:

- (a) The coupled bearing surfaces are identical;
- (b) The fluid is Newtonian;
- (c) No slippage occurs;
- (d) Negligible side leakage effect;
- (e) The condition is isothermal and steady-state.

3.1 TWO FLOW EQUATIONS FOR TWO DIFFERENT FLOW REGIMES

Where the continuum film is present, the multiscale mass flow rate through the bearing is calculated (per unit contact length) as in [14]:

$$q_m = \rho_{bf,1}^{eff} \left[\frac{F_1 h_{bf}^3}{6 \eta_{bf,1}^{eff}} \frac{dp}{dx} - \frac{h_{bf}^3}{\eta_{bf,1}^{eff}} \frac{dp}{dx} \left(1 + \frac{1}{2\lambda_{bf}} - \frac{q_0 - q_0^n}{q_0^{n-1} - q_0^n} \frac{\Delta_{n-2}}{h_{bf}} \right) \frac{\varepsilon}{1 + \frac{\Delta x}{D}} - u h_{bf} \right] - \rho \left\{ \frac{u}{2} h + \frac{h^3}{12\eta} \frac{dp}{dx} - \frac{h^3}{\eta_{bf,1}^{eff}} \frac{dp}{dx} \left[\frac{F_2 \lambda_{bf}^2}{6} - \frac{\lambda_{bf}}{1 + \frac{\Delta x}{D}} \left(\frac{1}{2} + \lambda_{bf} - \lambda_{bf} \frac{q_0 - q_0^n}{q_0^{n-1} - q_0^n} \frac{\Delta_{n-2}}{h_{bf}} \right) \right] \right\} \quad (1)$$

Equation (1) is then rearranged as:

$$\frac{dp}{dx} = \frac{ah+d}{ch^3+b} \quad (2)$$

where $a = u\rho/2$, $d = q_m + u\rho_{bf,1}^{eff} h_{bf}$,

$$b = \frac{\rho_{bf,1}^{eff} h_{bf}^3}{\eta_{bf,1}^{eff}} \left[\frac{F_1}{6} - \left(1 + \frac{1}{2\lambda_{bf}} - \frac{q_0 - q_0^n}{q_0^{n-1} - q_0^n} \frac{\Delta_{n-2}}{h_{bf}} \right) \frac{\varepsilon}{1 + \frac{\Delta x}{D}} \right] \quad (3)$$

$$c = \rho \left\{ \frac{1}{\eta_{bf,1}^{eff}} \left[\frac{F_2 \lambda_{bf}^2}{6} - \frac{\lambda_{bf}}{1 + \frac{\Delta x}{D}} \left(\frac{1}{2} + \lambda_{bf} - \lambda_{bf} \frac{q_0 - q_0^n}{q_0^{n-1} - q_0^n} \frac{\Delta_{n-2}}{h_{bf}} / D \right) \right] - \frac{1}{12\eta} \right\} \quad (4)$$

When there is only the adsorbed layer across the whole surface clearance, the nanoscale non-continuum flow equation gives that [15]:

$$q_m = \frac{S\rho_{bf,2}^{eff} h_{tot}^3}{12\eta_{bf,2}^{eff}} \frac{dp}{dx} - \frac{u}{2} h_{tot} \rho_{bf,2}^{eff} \quad (5)$$

Rearranging Eq. (5) gives that:

$$\frac{dp}{dx} = \frac{A}{h_{tot}^2} + \frac{Bq_m}{h_{tot}^3} \quad (6)$$

where $A = 6u\eta_{bf,2}^{eff}/S$ and $B = 12\eta_{bf,2}^{eff}/S\rho_{bf,2}^{eff}$.

3.2 NUMERICAL CALCULATION

Owing to the presence of the surface roughness, the problem is highly non-linear, and numerical calculation is mandatory for finding the solution. There are evenly distributed $(N+1)$ discretized points in the bearing inlet and outlet zones.

3.2.1 IN THE OUTLET ZONE

The pressure on the i^{th} discretized point in the outlet zone is expressed as:

$$\left. \frac{dp}{dx} \right|_i = \frac{p_i - p_{i-1}}{\delta_{x,o}} = \begin{cases} \frac{a_i h + d_i}{c_i h^3 + b_i}, & \text{for } h > 0 \\ \frac{A_i}{h_{tot,i}^2} + \frac{B_i q_m}{h_{tot,i}^3}, & \text{for } h_{tot,i} \leq 2h_{bf} \end{cases}, \text{ for } i=1, 2, \dots, N \quad (7)$$

where a_i, b_i, c_i, d_i, A_i and B_i : the values on the i^{th} discretized point, p_i and p_{i-1} the pressures on the i^{th} and $(i-1)^{th}$ discretized points in the outlet zone, respectively. The surface clearance, and the continuum film thickness on the i^{th} discretized point are expressed as:

$$h_{tot,i} = h_{tot,o} + R_z \sin(\omega x_i + \varphi) / 2 \text{ and } h = h_{tot,i} - 2h_{bf}, \delta_{x,o} = l_1 / N.$$

According to the boundary condition $p_0=0$, the discretized pressure was calculated by the following equation:

$$p_i = p_0 + \sum_{k=1}^i (p_k - p_{k-1}), \text{ for } i=1, 2, \dots, N \quad (8)$$

where $(p_k - p_{k-1})$ is calculated by Eq. (7).

Then following is obtained:

$$p_N = p_0 + \sum_{k=1}^N (p_k - p_{k-1}) \quad (9)$$

The film force per unit contact length contributed by the outlet zone is:

$$w_1 = \delta_{x,o} \left(\frac{p_N}{2} + \sum_{i=1}^{N-1} p_i \right) \quad (10)$$

3.2.2 IN THE INLET ZONE

The pressure on the i^{th} discretized point in the inlet zone is expressed as:

$$\left. \frac{dp}{dx} \right|_i = \frac{p_i - p_{i-1}}{\delta_{x,i}} = \begin{cases} \frac{a_i h + d_i}{c_i h^3 + b_i}, & \text{for } h > 0 \\ \frac{A_i}{h_{tot,i}^2} + \frac{B_i q_m}{h_{tot,i}^3}, & \text{for } h_{tot,i} \leq 2h_{bf} \end{cases}, \text{ for } i= N+1, N+2, \dots, 2N \quad (11)$$

where $\delta_{x,i} = l_2 / N$, and $h_{tot,i} = h_{tot,o} + (x_i - l_1) \tan \theta + R_z \sin(\omega x_i + \varphi) / 2$.

It is formulated that:

$$p_i = p_N + \sum_{k=N+1}^i (p_k - p_{k-1}), \text{ for } i = N+1, N+2, \dots, 2N \tag{12}$$

where $(p_k - p_{k-1})$ is calculated by Eq. (11).

The pressure on the $(2N)^{th}$ discretized point in the inlet zone is:

$$p_{2N} = p_N + \sum_{k=N+1}^{2N} (p_k - p_{k-1}) \tag{13}$$

The film force per unit contact length in the inlet zone is:

$$w_2 = \delta_{x,i} \left(\frac{p_N}{2} + \sum_{i=N+1}^{2N-1} p_i \right) \tag{14}$$

The carried load of the bearing is: $w = w_1 + w_2$.

3.2.3 NUMERICAL PROCEDURE

Figure 2 shows the numerical solution procedure that finally solved the value of Q_m . Then, all the discretized pressures can be calculated by the above equations. The convergence criterion is $|2(Q_{m,max} - Q_{m,min}) / (Q_{m,max} + Q_{m,min})| < 0.1\%$.

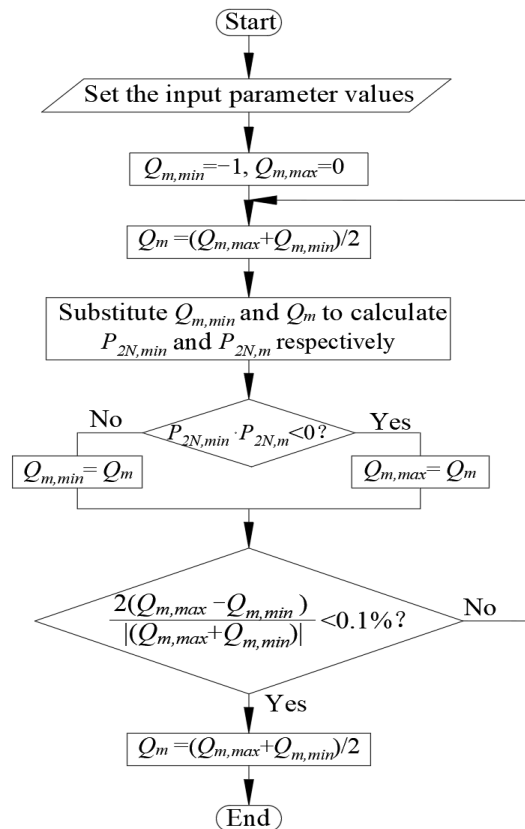


Fig. 2 The numerical solution procedure

We wrote by ourselves the computing program in the MATLAB tool according to the numerical procedure shown in Figure 2 to find the numerical solutions of the pressure distribution, the

surface separation distribution, and the carried load of the bearing for different operating conditions.

4. CALCULATION

The value of each parameter on the i^{th} discretized point $a_i, b_i, c_i, d_i, A_i, B_i$ are expressed as:

$$a_i = u\rho_i / 2, \quad d_i = q_m + u\rho_{bf,1,i}^{eff} h_{bf}, \quad A_i = 6u\eta_{bf,2,i}^{eff} / S, \quad B_i = 12\eta_{bf,2,i}^{eff} / S\rho_{bf,2,i}^{eff}$$

$$b_i = \frac{\rho_{bf,1,i}^{eff} h_{bf}^3}{\eta_{bf,1,i}^{eff}} \left[\frac{F_1}{6} - \left(1 + \frac{1}{2\lambda_{bf}} - \frac{q_0 - q_0^n}{q_0^{n-1} - q_0^n} \frac{\Delta_{n-2}}{h_{bf}} \right) \frac{\varepsilon}{1 + \frac{\Delta x}{D}} \right] \quad (15)$$

$$c_i = \rho_i \left\{ \frac{1}{\eta_{bf,1,i}^{eff}} \left[\frac{F_2 \lambda_{bf}^2}{6} - \frac{\lambda_{bf}}{1 + \frac{\Delta x}{D}} \left(\frac{1}{2} + \lambda_{bf} - \lambda_{bf} \frac{q_0 - q_0^n}{q_0^{n-1} - q_0^n} \frac{\Delta_{n-2}/D}{h_{bf}/D} \right) \right] - \frac{1}{12\eta_i} \right\} \quad (16)$$

By considering the fluid piezo-viscous and piezo-density effects, the relevant viscosities, and densities on the i^{th} discretized point are expressed as:

$$\eta_i = \eta_a \exp\{(\ln\eta_a + 9.67)[(1 + 5.1 \times 10^{-9} p_{i-1})^z - 1]\}, \quad \rho_i = \rho_a (1 + \beta \cdot p_{i-1})$$

$$\eta_{bf,1,i}^{eff} = C_{y1}(H_{bf,1}) \eta_a \exp\{(\ln\eta_a + 9.67)[(1 + 5.1 \times 10^{-9} p_{i-1})^z - 1]\}, \quad \rho_{bf,1,i}^{eff} = C_{q1}(H_{bf,1}) \rho_a (1 + \beta \cdot p_{i-1})$$

$$\eta_{bf,2,i}^{eff} = C_{y2}(H_{bf,2}) \eta_a \exp\{(\ln\eta_a + 9.67)[(1 + 5.1 \times 10^{-9} p_{i-1})^z - 1]\}, \quad \rho_{bf,2,i}^{eff} = C_{q2}(H_{bf,2}) \rho_a (1 + \beta \cdot p_{i-1})$$

where $z = \alpha / [5.1 \times 10^{-9} (\ln\eta_a + 9.67)]$, ρ_a is bulk density, η_a bulk viscosity of the fluid at ambient pressure, and α and β are constants.

The input parameter values are:

$$D = 0.5 \text{ nm}, \quad N = 5000, \quad u = 1 \times 10^{-6} \text{ m/s}, \quad \Delta_{n-2}/D = \Delta x/D = 0.15, \quad l_1 = l_2 = 100 \text{ um}, \quad \varphi = \pi, \quad \theta = 1 \times 10^{-4} \text{ rad}, \\ \alpha = 1.6 \times 10^{-8} \text{ m}^2/N, \quad \eta_a = 0.03 \text{ Pa}\cdot\text{s}, \quad \beta = 4 \times 10^{-10} \text{ Pa}^{-1}, \quad \omega = (\pi/5000) \text{ nm}^{-1}$$

The experimental measurements and the molecular dynamics simulation results of the rheological properties of the adsorbed molecular layers in the nanoscale surface separation correspond well, which shows the determining effect of the molecular-scale interaction strength between the fluid and the bearing surface. The important rheological parameters are shown as follows.

The parameters $C_{q1}(H_{bf,1})$ and $C_{q2}(H_{bf,2})$ are generally expressed as [16]:

$$C_q(H_{bf}) = \begin{cases} 1 & , \text{ for } H_{bf} \geq 1 \\ m_0 + m_1 H_{bf} + m_2 H_{bf}^2 + m_3 H_{bf}^3 & , \text{ for } 0 < H_{bf} < 1 \end{cases} \quad (17)$$

where H_{bf} is $H_{bf,1}$ or $H_{bf,2}$, $H_{bf,1} = h_{bf} / h_{cr,bf,1}$, $H_{bf,2} = h_{tot} / h_{cr,bf,2}$, m_0, m_1, m_2 , and m_3 are constants; $h_{cr,bf,1}$ and $h_{cr,bf,2}$ are, respectively, the critical thicknesses for characterizing the rheological properties of the adsorbed layers in the multiscale flow and in the nanoscale non-continuum flow.

$C_{y1}(H_{bf,1})$ and $C_{y2}(H_{bf,2})$ are formulated as [16]:

$$C_y(H_{bf}) = \begin{cases} 1 & , \text{ for } H_{bf} \geq 1 \\ a_0 + \frac{a_1}{H_{bf}} + \frac{a_2}{H_{bf}^2} & , \text{ for } 0 < H_{bf} < 1 \end{cases} \quad (18)$$

where H_{bf} is same as in Eq.(17), and a_0 , a_1 and a_2 are constants.

S is formulated as [16]:

$$S(H_{bf,2}) = \begin{cases} -1 & , \text{ for } H_{bf,2} \geq 1 \\ \left[n_0 + n_1(H_{bf,2} - n_3)^{n_2} \right]^{-1} & , \text{ for } n_3 < H_{bf,2} < 1 \end{cases} \quad (19)$$

where n_0 , n_1 , n_2 and n_3 are constants.

F_1 , F_2 and ε are as follows [14]:

$$F_1 = 0.18 \left(\frac{A_{n-2}}{D} - 1.905 \right) (\ln n - 7.897) \quad (20)$$

$$F_2 = (-3.707E - 4) \left(\frac{A_{n-2}}{D} - 1.99 \right) (n + 64) (q_0 + 0.19) (\gamma + 42.43) \quad (21)$$

$$\varepsilon = (4.56E - 6) \left(\frac{A_{n-2}}{D} + 31.419 \right) (n + 133.8) (q_0 + 0.188) (\gamma + 41.62) \quad (22)$$

h_{bf} is calculated as:

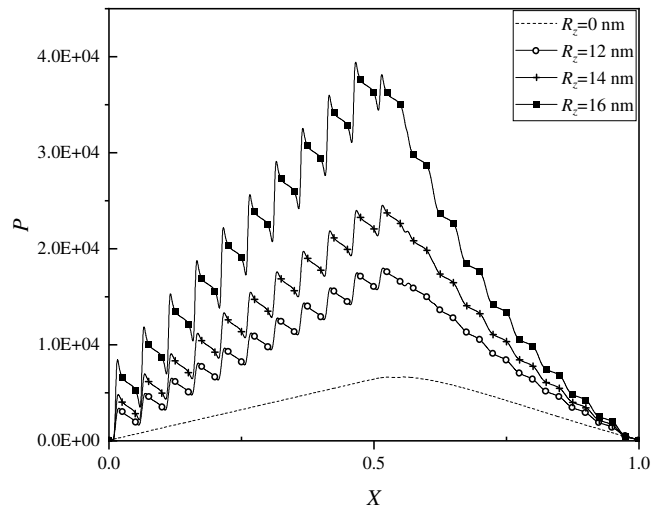
$$h_{bf} = nD + \frac{q_0 - q_0^n}{q_0^{n-1} - q_0^n} A_{n-2} \quad (23)$$

The parameter values for the weak, medium and strong fluid-bearing surface interactions are shown in Refs. 13 and 16 and therefore not repeated.

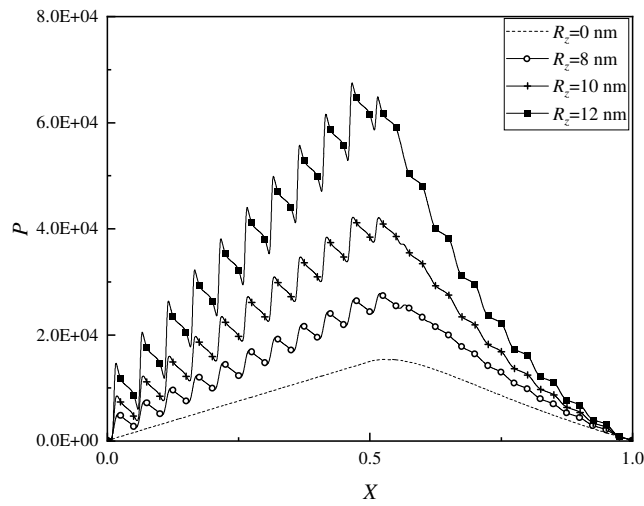
5. RESULTS

5.1 DIMENSIONLESS HYDRODYNAMIC PRESSURES

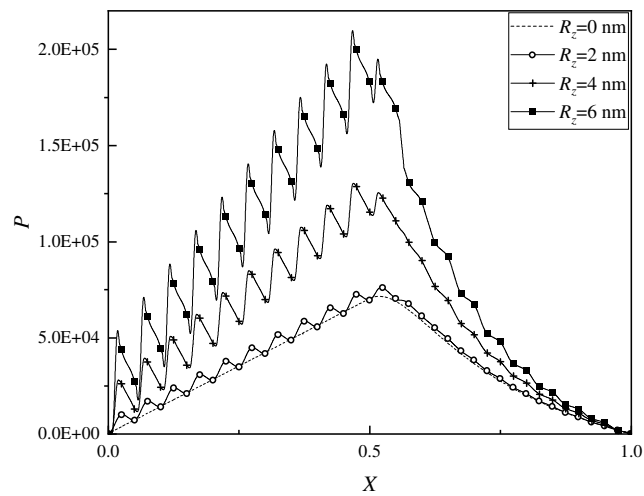
The hydrodynamic pressure in the bearing is shown to be increasing with the surface roughness in Figures 3(a-c). The surface roughness effect is stronger if the fluid-bearing surface interaction is stronger. For the weak interaction, the nanoscale surface roughness, such as $R_z=16 \text{ nm}$, increases the hydrodynamic pressure by more than 3 times in comparison to the smooth surface results ($R_z=0 \text{ nm}$). For the strong interaction, the surface roughness $R_z=6 \text{ nm}$ gives the same increasing effect.



(a) For the weak interaction



(b) For the medium interaction

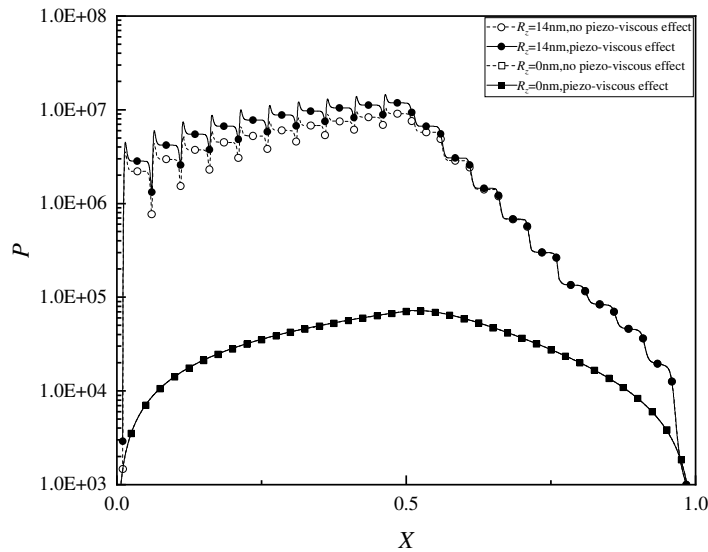


(c) For the strong interaction

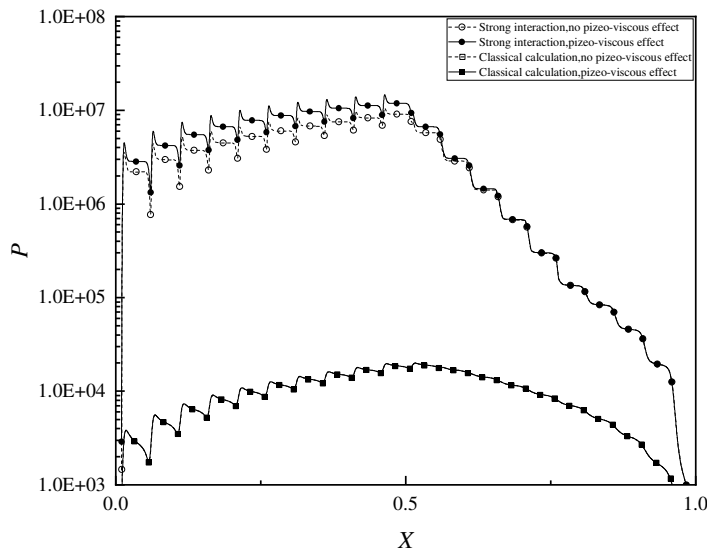
Fig. 3 Dimensionless pressure distributions in the bearing when $h_{tot,0} = 10 \text{ nm}$ and $\theta = 1 \times 10^{-4} \text{ rad}$

Figure 4 (a) shows that for the strong interaction, the hydrodynamic pressures are so low that the piezo-viscous effect on the pressure is negligible when the stationary surface is perfectly smooth (i.e., $R_z=0\text{ nm}$). However, the surface roughness $R_z=14\text{ nm}$ increases the hydrodynamic pressure by 2 orders, so the piezo-viscous effect further significantly increases the hydrodynamic pressure.

Figure 4 (b) shows that for $R_z=14\text{ nm}$, the classical calculation (ignoring the adsorbed layer and assuming the Newtonian fluid) results in the pressure so low that the piezo-viscous effect is negligible. The present calculation with the strong interaction results in the pressures nearly 3 orders higher than the classical calculation, so the piezo-viscous effect is significant.



(a) For the strong interaction



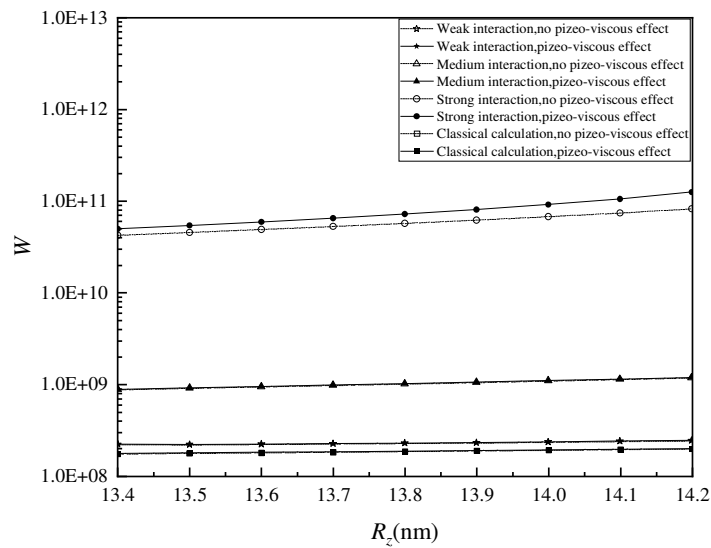
(b) $R_z=14\text{ nm}$

Fig. 4 Piezo-viscous effect for different surface roughness and different interactions for $h_{tot,0}=10\text{ nm}$ and $\theta=1\times 10^{-4}\text{ rad}$

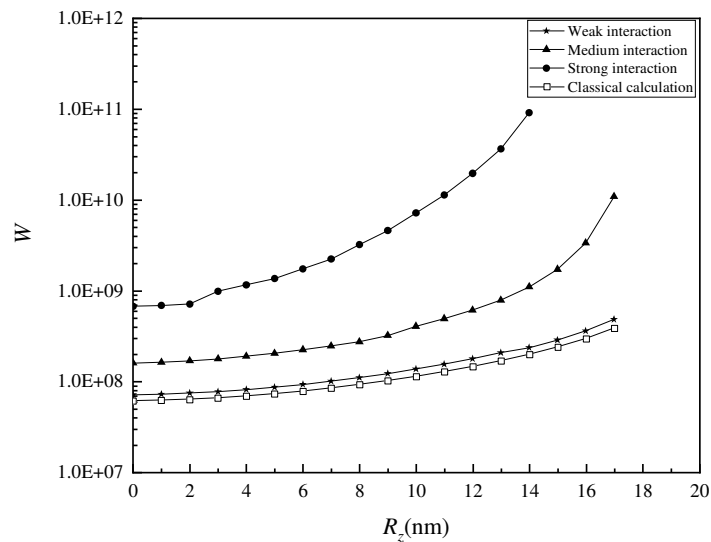
5.2 LOAD OF THE BEARING

Figure 5 (a) shows that for the weak and medium interactions, the piezo-viscous effect on the carried load of the bearing is negligible when $h_{tot,o} = 10 \text{ nm}$, $\theta = 1 \times 10^{-4} \text{ rad}$, and R_z is below 14 nm . However, for the strong interaction, in the same operating conditions, the piezo-viscous effect considerably increases carried load of the bearing particularly for higher surface roughness.

Figure 5 (b) shows that the classical calculation also gives the increase in the bearing load when the surface roughness is higher. However, this increase is higher for a stronger interactions. For the strong interaction and the surface roughness $R_z = 14 \text{ nm}$, the resulting bearing load is nearly 3 orders larger than the classical calculation.



(a)



(b)

Fig. 5 Dimensionless carried loads of the bearing when $h_{tot,o} = 10 \text{ nm}$ and $\theta = 1 \times 10^{-4} \text{ rad}$

6. CONCLUSIONS

The surface roughness effect in the hydrodynamic thrust bearing with ultra-low clearance is investigated with the multiscale approach. The adsorbed layer effect is incorporated, and the surface roughness is limited to the 1nm scale. Numerical calculations were made, and the conclusions are as follows:

- The hydrodynamic pressure and the bearing load are enhanced with the surface roughness increase. The stronger the fluid-bearing surface interaction, the greater the enhancement.
- For the strong interaction or/and high surface roughness, the fluid piezo-viscous effect must be incorporated.
- For evaluating the hydrodynamic thrust bearing with ultra/low clearance correctly, the surface roughness and the adsorbed layer must be considered simultaneously. The lubrication status in the bearing is quite complicated. The multiscale analysis and numerical calculation for this model of bearing are mandatory.

7. NOMENCLATURE

a_0, a_1, a_2 - constant

C_{y1} - $\eta_{bf,1}^{eff} / \eta$

C_{q1} - $\rho_{bf,1}^{eff} / \rho$

C_{y2} - $\eta_{bf,2}^{eff} / \eta$

C_{q2} - $\rho_{bf,2}^{eff} / \rho$

D - fluid molecule diameter

h - continuum film thickness

$h_{cr,bf,1}$ - critical thickness for characterizing the rheological properties of the adsorbed layer in the multiscale flow

$h_{cr,bf,2}$ - critical thickness for characterizing the rheological properties of the adsorbed layer in the nanoscale non-continuum flow

h_{bf} - adsorbed layer thickness

h_{tot} - surface separation

$h_{tot,o}$ - surface separation on the exit of the bearing

$H_{bf,1}$ - $h_{bf} / h_{cr,bf,1}$

$H_{bf,2}$ - $h_{tot} / h_{cr,bf,2}$

l_1, l_2 - widths of the outlet and inlet zones, respectively

$m_0, m_1, m_2, m_3, n_0, n_1, n_2, n_3$ - constant

n - equivalent number of the fluid molecules across the adsorbed layer thickness

- $N+1$ - number of the discretized points in the outlet or inlet zones
- p - hydrodynamic pressure
- P - dimensionless pressure, $ph_{tot,o} / u\eta_a$
- q_0 - Δ_{j+1} / Δ_j
- q_m - total mass flow rate per unit contact length through the bearing
- Q_m - dimensionless total mass flow rate, $q_m / (uh_{tot,o}\rho_a)$
- R_z - maximum height of the rough surface profile
- S - parameter accounting for the non-continuum effect of the adsorbed layer confined in the whole surface separation
- u - sliding speed of the bearing
- w_1, w_2 - load components contributed by the outlet and inlet zones, respectively
- W - dimensionless load, $w / u\eta_a$
- x - coordinate
- X - dimensionless coordinate, $x / (l_1 + l_2)$
- θ - wedge angle of the bearing
- γ - exponent
- ρ - fluid bulk density
- ρ_a - fluid bulk density at ambient pressure
- $\rho_{bf,1}^{eff}$ - average density of the adsorbed layer in the multiscale flow
- $\rho_{bf,2}^{eff}$ - average density of the adsorbed layer in the nanoscale non-continuum flow
- η - fluid bulk viscosity
- η_a - fluid bulk viscosity at ambient pressure
- $\eta_{bf,1}^{eff}$ - effective viscosity of the adsorbed layer in the multiscale flow
- $\eta_{bf,2}^{eff}$ - effective viscosity of the adsorbed layer in the nanoscale non-continuum flow
- $\eta_{line,j-1}$ - local viscosity between the j^{th} and $(j-1)^{th}$ fluid molecules across the adsorbed layer thickness
- λ_{bf} - h_{bf} / h
- Δ_j - separation between the $(j+1)^{th}$ and j^{th} fluid molecules across the adsorbed layer thickness
- Δx - separation between the neighbouring fluid molecules in the flow direction in the adsorbed layer
- Δ_{n-2} - separation between the neighbouring fluid molecules across the adsorbed layer thickness just on the boundary between the adsorbed layer and the continuum fluid film

$\delta_{x,o}$ - distances between two neighbouring discretized points in the outlet zone, l_1 / N

$\delta_{x,i}$ - distances between two neighbouring discretized points in the inlet zone, l_2 / N

8. REFERENCES

- [1] H. Iliev, Failure analysis of hydro-generator thrust bearing, *Wear*, Vol. 225-229, pp. 913-917, 1999. [https://doi.org/10.1016/S0043-1648\(98\)00410-4](https://doi.org/10.1016/S0043-1648(98)00410-4)
- [2] O.V. Antonova, A.I. Borovkov, Y.Y. Boldyrev, I.B. Voynov. Variational problem for hydrogenerator thrust bearing, *Materials Physics and Mechanics*, Vol. 34, pp.97-102, 2017.
- [3] L. Zhai, Y. Luo, Z. Wang, X. Liu, Y. Xiao, A review on the large tilting pad thrust bearings in the hydropower units, *Renewable and Sustainable Energy Reviews*, Vol. 69, pp.1182-1198, 2017. <https://doi.org/10.1016/j.rser.2016.09.140>
- [4] C.I. Papadopoulos, E.E. Efstathiou, P.G. Nikolakopoulos, L. Kaiktsis, Geometry Optimization of Textured 3-D Micro-Thrust Bearings, *ASME Turbo Expo: Turbine Technical Conference and Exposition*, Vol. 3, pp. 801-810, 2011.
<https://doi.org/10.1115/1.4004990>
- [5] D.Y.C. Chan, R.G. Horn, The drainage of thin liquid films between solid surfaces, *Journal of Chemical Physics*, Vol. 83, pp. 5311-5324, 1985. <https://doi.org/10.1063/1.449693>
- [6] O. Atkas, N.R. Aluru, A combined continuum/DSMC technique for multiscale analysis of microfluidic filters, *Journal of Computational Physics*, Vol. 178, pp. 342-372, 2002.
<https://doi.org/10.1006/jcph.2002.7030>
- [7] T.H. Yen, C.Y. Soong, P.Y. Tzeng, Hybrid molecular dynamics-continuum simulation for nano/mesoscale channel flows, *Microfluidics and Nanofluidics*, Vol. 3, pp. 665-675, 2007.
<https://doi.org/10.1007/s10404-007-0154-7>
- [8] C. Liu, Z. Li, On the validity of the Navier-Stokes equations for nanoscale liquid flows: The role of channel size, *AIP Advances*, Vol. 1, No. 1, pp. 032108, 2011.
<https://doi.org/10.1063/1.3621858>
- [9] J.J. Magda, M. Tirrell, H.T. Davis, Molecular dynamics of narrow, liquid-filled Pores, *Journal of Chemical Physics*, Vol. 83, pp. 1888-1901, 1985.
<https://doi.org/10.1063/1.449375>
- [10] E. Meyer, R.M. Overney, K. Dransfeld, T. Gyalog, Nanoscience: Friction and Rheology on the Nanometer Scale, *World Scientific Press, New Jersey*, 1998.
<https://doi.org/10.1142/3026>
- [11] M. Grosse-Rhode, G.H. Findenegg, Formation of ordered monolayers of n-alkanes at the cleavage face of nickel chloride, *Journal of Colloid and Interface Science*, Vol. 64, No. 2, pp. 374-376, 1978. [https://doi.org/10.1016/0021-9797\(78\)90375-2](https://doi.org/10.1016/0021-9797(78)90375-2)
- [12] Y.B. Zhang, New explanation for the measured very low film thicknesses in lubricated concentrated contacts, *Journal of the Balkan Tribological Association*, Vol. 27, No. 3, pp. 439-444, 2021.

- [13] C. Wang, Y.B. Zhang, Analysis for hydrodynamic wedge-platform thrust bearing with ultra low surface separation, *International Journal of Rotating Machinery*, Vol. 2022, pp. 1-17, 2022. <https://doi.org/10.1155/2022/8101357>
- [14] Y.B. Zhang, Modeling of flow in a very small surface separation, *Applied Mathematical Modelling*, Vol. 82, pp. 573-586, 2020. <https://doi.org/10.1016/j.apm.2020.01.069>
- [15] Y.B. Zhang, The flow equation for a nanoscale fluid flow, *International Journal of Heat and Mass Transfer*, Vol. 92, pp. 1004-1008, 2016. <https://doi.org/10.1016/j.ijheatmasstransfer.2015.09.008>
- [16] Y.B. Zhang, Modeling of molecularly thin film elastohydrodynamic lubrication, *Journal of the Balkan Tribological Association*, Vol. 10, No. 3, pp. 394-421, 2004.